Published in final edited form as:
Neuroimage. 2014 April 1; 89: 262–270. doi:10.1016/j.neuroimage.2013.11.052.

MR Vascular Fingerprinting: A New Approach to Compute Cerebral Blood Volume, Mean Vessel Radius, and Oxygenation Maps in the Human Brain

T. Christen[1,*], **NA. Pannetier**[2,3,*], **W. Ni**[1], **D. Qiu**[1], **M. Moseley**[1], **N. Schuff**[2,3], and **G. Zaharchuk**[1]

[1]Department of Radiology, Stanford University, Stanford, California, USA

[2]Center for Imaging of Neurodegenerative Diseases, Veterans Affairs Medical Centre, San Francisco, USA

[3]Department of Radiology and Biomedical Imaging, University of California San Francisco, San Francisco, CA, USA

Abstract

In the present study, we describe a fingerprinting approach to analyze the time evolution of the MR signal and retrieve quantitative information about the microvascular network. We used a Gradient Echo Sampling of the Free Induction Decay and Spin Echo (GESFIDE) sequence and defined a fingerprint as the ratio of signals acquired pre and post injection of an iron based contrast agent. We then simulated the same experiment with an advanced numerical tool that takes a virtual voxel containing blood vessels as input, then computes microscopic magnetic fields and water diffusion effects, and eventually derives the expected MR signal evolution. The parameters inputs of the simulations (cerebral blood volume [CBV], mean vessel radius [R], and blood oxygen saturation [SO2]) were varied to obtain a dictionary of all possible signal evolutions. The best fit between the observed fingerprint and the dictionary was then determined using least square minimization. This approach was evaluated in 5 normal subjects and the results were compared to those obtained using more conventional MR methods, steady-state contrast imaging for CBV and R and a global measure of oxygenation obtained from the superior sagittal sinus for SO2. The fingerprinting method enabled the creation of high-resolution parametric maps of the microvascular network showing expected contrast and fine details. Numerical values in gray matter (CBV=3.1±0.7%, R=12.6±2.4μm, SO2=59.5±4.7%) are consistent with literature reports and correlated with conventional MR approaches. SO2 values in white matter (53.0±4.0%) were slightly lower than expected. Numerous improvements can easily be made and the method should be useful to study brain pathologies.

Corresponding author: Name: Thomas Christen, Mailing address: Lucas center for Imaging, Stanford University, 1201 Welch Rd., Mailcode 5488, Stanford, CA 94305-5488, Telephone number: +1 650-723-5393, christenthomas@yahoo.fr.
*Authors contributed equally

Disclosures: None

Keywords

Magnetic Resonance Imaging; Fingerprint; Numerical Simulation; Cerebral Blood Volume; Vessel Size Imaging; Blood Oxygen Saturation

Introduction

The amount of blood in a voxel, the geometry of the blood vessels, and the level of blood oxygenation all together can impact the MR signal time evolution in both gradient and spin echo experiments. This differing response of the MR signal evolution is the basis of the blood-oxygen level dependent (BOLD) effect, which depends on magnetic susceptibility variations induced by the paramagnetic effect of deoxyhemoglobin (Ogawa et al., 1990). All these parameters contributing to BOLD are potentially important biomarkers for studying angiogenesis or hypoxic processes in pathologies such as cancer (Carmeliet and Jain, 2000; Vaupel and Mayer, 2007) or stroke (Sobesky et al., 2005). Equally important is the differentiation between the individual contributions of these parameters to BOLD images. Variations of the microvascular characteristics have also been reported in neurodegenerative diseases (Hunter et al., 2012) and psychological disorders (Rigau et al., 2007).

The BOLD effect is, however, complex and only a few methods have tried to extract quantitative information from baseline experiments rather than looking at relative variations of the signal. Quantitative BOLD approaches (An and Lin, 2000; He and Yablonskiy, 2007) aim to measure venous blood oxygen saturation and cerebral blood volume fraction (CBV) by analyzing the formation of the spin echo signal using a mathematical model. While the results have been encouraging, recent studies (Dickson et al., 2011) have shown that the existing analytical models can be inaccurate in describing the BOLD signal due to the difficulty in parameterizing the complex influence of the water diffusion process. Separating the effects of CBV and blood oxygenation on the signal time evolution is also extremely challenging (Sedlacik and Reichenbach, 2010). In previous works, we proposed to measure separately some parameters of the model and to reduce the effect of diffusion by observing only the free induction decay (FID) (Christen et al., 2012, 2010). Yet, low blood oxygenation estimates in white matter suggest that this approach still need refinements.

A powerful alternative to analytical modeling has been recently proposed (Ma et al., 2013), in which numerical simulations of the MRI signal are used in conjunction with the concept of fingerprinting. In the first demonstration of the method, a fast MR sequence (inversion-recovery balanced free precession sequence (IR-bSSFP)) known for its sensitivity to relaxation times (T1 and T2) was used to acquire data *in vivo*. The acquisition was repeated with a random choice of parameters such as repetition time, flip angle, and inversion time, resulting in a different signal evolution in every voxel. The signal was too complex to be analyzed with classic MR equations, yet this ‘fingerprint’ was compared to a dictionary of curves obtained using numerical simulations of the same experiment. Using this approach, simultaneous measurements of T1, T2, frequency, and proton density were obtained with good accuracy and robust behavior in the presence of noise and other acquisitions errors.

In the present study, we hypothesize that a similar approach of using numerical simulations and MRI fingerprinting together in an analysis of FID and SE signal evolutions can be used to retrieve quantitative information about the microvascular network. As a demonstration, we sampled the MR signal evolution with a Gradient Echo Sampling of the FID and SE (GESFIDE) sequence (Fig.1c) and defined the vascular fingerprint as the ratio of GESFIDE signal acquired pre and post contrast agent injection. We then simulated the same experiment with a numerical tool that takes a virtual voxel containing blood vessels as input,

computes the microscopic magnetic fields and water diffusion effects, and eventually predicts the MR signal evolution. The parameter inputs of the simulations (CBV, vessel radius, and blood oxygenation) were varied to obtain a dictionary of possible MR signal evolutions. The fingerprint and dictionary were finally compared using a least square minimization method. Our approach was tested in normal human subjects and the results were compared to conventional MR vascular imaging approaches.

Materials and Methods

Patient Population

This study was approved by the institutional review board of Stanford Medical School and was Health Insurance Portability and Accountability Act (HIPAA) compliant. Five normal subjects (3 men, 2 women; mean age 36 years; range 27-61 years) were included in the study after giving informed written consent.

Imaging Protocol

MRI data were acquired using a 3.0 T scanner (MR750, GE Healthcare, Waukesha, WI, USA) and an 8-channel receive-only head coil. A 3D T1-weighted fast spoiled gradient echo sequence (TR=9.2ms, TE=3.7ms, FOV=22×22cm^2, slice thickness ST=1.2mm, acquisition matrix =256×256, 130 slices) was used to acquire high-resolution anatomical information of the whole brain. The 2D GESFIDE sequence (TR=2000ms, 40 echoes (14 acquired before the 180 degree pulse), echo spacing ΔTE=3ms, Spin echo SE=100ms, FOV=20×20cm^2, ST=1.5mm, 128×128, 12 interleaved slices with 1 mm spacing, Tacq=4min) was acquired pre- and 2 minutes post-injection of ferumoxytol (17mL at 1 mL/s, Fe 30 mg/mL, Feraheme, AMAG Pharmaceuticals Inc., Cambridge, MA, USA). The slices covered 1.8 cm in craniocaudad dimension at the level of the lateral ventricles, which optimally included both deep and cortical gray matter (GM), white matter (WM), and cerebrospinal fluid (CSF).

Data were imported into Matlab (MathWorks Inc., Natick, MA, USA) for post-processing, and SPM8 (Wellcome Department of Imaging Neuroscience, UCL, London, England) was used to co-register the parametric maps and the anatomical scan. FSL BET (FMRIB, Oxford, UK) was used for brain extraction and an Otsu's 3-thresholding approach (Otsu, 1979) was applied to segment WM, GM, and CSF. To increase the SNR of the GESFIDE data, two slices were averaged (equivalent to 3mm slice thickness) and a 2D spatial Gaussian smoothing was applied (support 3×3, width 0.5).

MR Signal Numerical Model

The MR signal was simulated with a 2D numerical approach that models the effects of water protons diffusing in magnetic field gradients. We briefly outline here the principal components of the simulation tool. In the following, bold capital letters refers to 2D-lattices, × to the point wise multiplication and ⊗ to the convolution. Details of the model can be found in (Pannetier et al., 2013b).

The vessels were modeled by N=96 magnetic circular inclusions of radius R that were randomly distributed on a square lattice with a periodic boundary condition. These vessels occupied CBV and the lattice spatial extent was adapted accordingly. The magnetic susceptibility difference, $\Delta\chi$, between the vessels and the surrounding tissue was given by the oxygenation saturation level (SO2) according to: $\Delta\chi = \Delta\chi_0.\mathrm{Hct}.(1 - \mathrm{SO2})$ where $\Delta\chi_0$=0.264ppm (CGS units, (Spees et al., 2001)) the magnetic susceptibility difference between fully deoxygenated and fully oxygenated red blood cells. In the study, a constant hematocrit of 0.42 was used for all subjects. Because our numerical voxels represent the

microvascular network, we used a ratio of 0.85 (Eichling et al., 1975) to convert the large vessel Hct to small vessel Hct. Thus Hct was set to 0.42*0.85=0.36.

At each time step δt, changes in the lattice of the magnetization moments were simulated using a deterministic iterative approach that models the effects of water diffusion and the rotational effects induced by the local magnetic field perturbations, **ΔB**, and the RF pulses. The spin-spin relaxations of the tissue and blood compartments were disregarded in the simulation because their effect cancels out when generating the vascular fingerprint (see Fingerprint Generation and Recognition paragraph below). The magnetic field perturbations were computed using the Fourier based approach introduced in (Marques and Bowtell, 2005; Salomir et al., 2003) and adapted here in 2D (Pannetier et al., 2013a). The diffusion effect was modeled by the convolution of the magnetization lattice with a discrete Gaussian kernel denoted **D** (Bandettini and Wong, 1995; Klassen and Menon, 2007; Lindeberg, 1990). Free exchanges of water at the blood vessel walls were considered. At each δt, the changes in the complex transverse magnetization lattice $\mathbf{M}_{\perp}$ were computed according to:

$$\boldsymbol{M}t+\delta t=(\boldsymbol{M}t\times\exp(-i\gamma\boldsymbol{\Delta B}\delta t))\otimes\boldsymbol{D}$$

where γ the gyromagnetic ratio of protons. The MR signal was calculated at each δt by summing the complex values of the lattice **M**.

Specific simulation parameters were as follows: The step time of the simulation was set to δt=0.5ms. The lattices were defined on 256×256 points. Diffusion kernel extend was characterized by the apparent water diffusion coefficient D_{H20}=800μm^2.s^{-1} (Bihan, 2013). Convolutions were performed in the Fourier space to reduce the computational cost and to benefit from the folding effect at the border of the geometry.

Dictionary

A dictionary of MR signal evolutions was generated by simulating the GESFIDE sequence with the numerical model and by varying the vascular properties of the virtual voxels within a physiological range defining a four-dimensional space along R, CBV, SO2, and time. The parameter space was sampled non-uniformly to focus the dictionary on the most likely physiological values: R = [1-(.25)-5-(.5)-10-(1)-15-(2)-25]μm, CBV = [.5-(.25)-2-(.1)-4-(.25)-8-(.5)-10-(1)-15-(2)-25]% and SO2 = [0-(10)-50-(2.5)-100]% (with the increment in brackets). A subset of the dictionary is displayed in Figure 1b.

The dictionary corresponding to the MR signal prior to injection was identical for all volunteers. On the contrary, the dictionary of the MR signals after injection was simulated individually for each volunteer with the magnetic susceptibility increase, $\Delta\chi_{inj}$, due to the contrast agent injection. The increase of $\Delta\chi_{inj}$ was computed based on the total blood volume (TBV) of the volunteer, the Ferumoxytol dose (m_{Fe}= 0.510g) and the saturation magnetization of iron, M_{sat}=0.396 μT/mmol of iron (Troprès et al., 2001) according to:

$$\Delta\chi_{\mathrm{inj}}=\mathrm{m}_{\mathrm{Fe}}/\mathrm{M}_{\mathrm{Fe}}/\mathrm{TBV}\times\mathrm{M}_{\mathrm{sat}}/\mathrm{B}_0.$$

with M_{Fe} the standard atomic weight of iron and B_0 the magnitude of the main magnetic field. The TBV was computed using the Gilcher's rule of five (McLeod et al., 2010) using the patient's weight, as listed in Table 1.

Each dictionary consisted of 52920 individual simulations. The computation was performed in the Matlab environment using the Matlab Distributed Computing Server deployed on a 24-nodes cluster. The parallel building of a single dictionary took about 12 hrs.

Fingerprint Generation and Recognition

The vascular fingerprints were generated by taking the ratio of post- and pre-contrast GESFIDE signals (Fig. 1d) thereby minimizing the effects of static MRI effects, such as spin-spin relaxation, B_0 inhomogeneity, B_1 inhomogeneity, and imperfect refocusing. A dictionary of possible vascular fingerprints was built for each subject by taking the ratio of the individual specific post- and pre-contrast dictionaries. Each new dictionary was subsequently resampled along the temporal dimension using cubic spline interpolation to match the acquisition time of the GESFIDE signal. Prior to the recognition, the dictionary and the fingerprints were normalized by dividing each element by their mean value. This allows for compensating the different scaling factor between the simulations and the MR signal acquisitions.

For each voxel, the normalized vascular fingerprint was compared to the normalized dictionary signals by computing the coefficients of determination r^2. The highest coefficient was selected and the corresponding CBV, SO2, and R values from the simulations were retrieved to obtain the parametric maps. A coefficient $r^2 < 0.5$ was considered no match and the corresponding voxel was not displayed in the parametric maps.

To investigate the robustness and the uniqueness of the solution, the characteristics of the dictionaries were evaluated by computing the root mean square deviation (RMSD) between one reference curve and all other signal evolutions. The reference MR signal was chosen to match physiological values with: R=3μm, CBV=3% and SO2=65%. Two dictionaries of curves were analyzed for comparison: a dictionary generated from the normalized MR signal prior to the contrast agent injection and a dictionary generated from the normalized ratio Post/Pre.

Steady-State CBV & Relative Vessel Radius

Changes in transverse relaxation rates were calculated voxel-by-voxel from GESFIDE signal intensities pre (S_{pre}) and post injection (S_{post}) of the contrast agent:

$$\Delta R_2^* = 1/TE \cdot \ln(S_{pre}(TE)/S_{post}(TE))$$

The 10th gradient echo image (TE=31.5ms, maximum BOLD sensitivity at 3T (Krüger et al., 2001)) was used for ΔR_2^* and the spin echo image (TE=100ms) for ΔR_2. SS_CBV was then estimated using the steady-state approach described by (Troprès et al., 2001):

$$SS\_CBV = 3/(4\pi\gamma\Delta\chi_{USPIO}B_0) \cdot \Delta R_2^*$$

The ratio $\Delta R_2^*/\Delta R_2$ was taken as an approximation of the relative vessel radius (Dennie et al., 1998).

Global Sagittal Sinus Oximetry

MR susceptometry (Fernández-Seara et al., 2006) was used for global brain oxygenation measurements. The phase signal of the first 10 gradient echo images was temporally unwrapped and a linear fit of the phase evolution was used to derive a magnetic field map. The superior sagittal vein and its surrounding tissue were manually delineated in 3 slices per

volunteer. The following equation was then applied to derive global venous blood oxygenation (SvO2):

$$|Bv - Bs| = \frac{4}{3}\pi\Delta\chi_0 Hct(1 - SvO_2)B_0$$

where Bv and Bs are the average magnetic field inside the superior sagittal vein (considered here as infinitely long cylinder oriented parallel to B0) and the surrounding tissue respectively. Hct and $\Delta\chi_0$ values were taken as previously described in numerical model description section.

Statistics

To obtain robust group estimates of the vascular relationships (i.e. CBV vs ΔR_2*, CBV vs SS_CBV and Radius vs ΔR_2*/ΔR_2) while also accounting for the inter-subject variability, we designed a linear mixed effects model with random variations of intercepts and slopes for each subject. The mixed effects analysis was done using the lme4 package in R (R – The Project of Statistical Computing http://www.r-project.org/). To test whether the relationships are significant we compared the full model with the fixed effect against one without the fixed effect using maximum likelihood tests and reported the results in term of p value and $\chi^2(d)$ with d the number of degrees of freedom.

The relationship between SO2 vs SvO2 in the gray matter was analyzed using a linear model. r^2 was evaluated to characterize the fit quality.

Results

Uniqueness and Robustness

Figure 2 displays three orthogonal planes of the RMSD between the reference signal and all other signals in two different dictionaries. The planes intersect at the coordinates matching the reference MR signal (white arrows, RMSD = 0, R=3μm, CBV=3% and SO2=65%). In Fig. 2(a-c), the RMSD from the dictionary prior to the contrast agent injection exhibits long, narrow valleys of minima, which extend far beyond the point representing the reference curve. This result is in agreement with previous studies that measured blood oxygenation without contrast agent (Sedlacik and Reichenbach, 2010; Sohlin and Schad, 2011) and demonstrates that the simultaneous estimation of CBV and SO2, and to a lesser extent the radius, is challenging due to the similarity of the MR signal evolutions.

In contrast, the RMSD calculated from the dictionary Post/Pre ratio exhibits relatively local minima centered around the reference signal (Fig. 2d-f). This minimum is highly localized for the radius and the CBV (Fig. 2f) whereas it has a larger extent along the SO2 dimension (Fig. 2d-e). This suggests a higher accuracy for the estimation of radius and CBV than for the estimation of SO2.

We then investigated the reliability of the pattern matching process by applying the approach to a subset of noisy simulated vascular fingerprints from the dictionary. We considered 4680 fingerprints scattered over R=[1-14]μm, CBV=[0.5-12]% and SO2=40-100]%. Gaussian white noise was added to these theoretical fingerprints. A noise level equivalent to an SNR=70 was used in all experiments in agreement with the SNR observed in the *in vivo* data when evaluated at the spin-echo time and after smoothing. The estimated R, CBV, and SO2 were measured by matching the simulated noisy fingerprints to the original dictionary. Results are shown in Fig. 3 as box-and-whisker plots. All plots present a linear relationship between the estimated and the theoretical values but accuracy

varies between parameters. Across the studied range, estimations of CBV are the most accurate (4% mean absolute relative error) followed by estimates of R (9% relative error), whereas estimates of SO2 have a substantially lower reliability (21% relative error).

Parametric Maps

Fig. 4 presents an example of GESFIDE images and different MR vascular fingerprints. Images at different echo times and prior and after contrast agent injection are shown on Fig. 4a. The impact of the contrast agent is clearly visible at all echo times and large vessels can be distinguished at longer echo times. On Fig. 4b, normalized vascular fingerprints averaged over gray matter and white matter ROI are presented. The difference in these fingerprints suggests a difference in the underlying vascular features. Fig. 4c presents an example of a vascular fingerprint data obtained in a gray matter voxel. The best match obtained from the dictionary is overlaid with the corresponding vascular parameters. The agreement between the data and the dictionary is strong (r^2=0.95).

Representative parametric maps of one of the volunteers (#4 with overall the best r^2) are presented in Fig.5. CBV maps show a good contrast between GM and WM, while mean vessel radius and SO2 maps are more homogeneous. The fit quality maps shows low values only in CSF, low SNR white matter regions, and highly vascularised area such as the superior sagittal sinus vein. The numerical values averaged over the volunteers are CBV=3.1±0.7%, R=12.6±2.4μm, SO2=59.5±4.7% in GM and CBV=1.9±0.4%, R=12.7±2.1μm, SO2=53.0±4.0% in WM. Individual estimates of the parameters are provided in Table1. Exquisite CBV contrasts in deep white matter regions are also observed (white arrows) suggesting higher vasculature in this area, corresponding to the medullary veins of the deep white matter. This observation is supported by the larger radii measured in the same regions in the vessel radius maps (blue arrows).

Comparison to Alternative Imaging Approaches

Scatterplots of the different parameters against results from alternative approaches are presented in Fig. 6. The data correspond to white matter (squares) and gray matter (triangles) regions of interest averaged in the 5 central slices in each healthy volunteer (colors). In Fig. 6a-c, fixed effect equation and fits for each volunteer are represented. Fig. 6a shows CBV values against ΔR2*. A linear relationship with ΔR2* is found with a high significance ($\chi^2(1)=12.26$, $p=5.10^{-4}$). The comparison with steady-state CBV values (Fig. 6b) shows high significance ($\chi^2(1)=26.73$, $p=2.10^{-7}$) but with reduced CBV values compared to steady-state CBV by about 38%. The variation in the individual slopes is strongly reduced compared to the ones found in Fig. 6a (3% vs 150% relative standard deviation in the slopes) suggesting that this variation is mainly due to variation in $\Delta\chi_{inj}$. In Fig. 6c, comparison of vessel radius vs ΔR2*/ΔR2 shows higher residuals between the data and the model compared to CBV plots. In some subjects, a discrepancy between WM and GM is also observed. The correlation is still highly significant ($\chi^2(1)=12.66$, $p=4.10^{-4}$). It is also worthwhile to notice that the relation of R vs ΔR2*/ΔR2 has been shown to be slightly non-linear (Jochimsen et al., 2010). Values of SO2 in GM were strongly correlated (r^2 = 0.984) to global sagittal sinus oxygen saturation (Fig. 6d).

Discussion

This study demonstrates that quantitative information of important vascular parameters can be obtained with an MR fingerprinting approach. Analyzing the MR signal evolution, we obtained high-resolution parametric maps of CBV, vessel radius, and blood oxygen saturation in the human brain.

The contrast in our CBV maps are consistent with reports from MR studies using dynamic susceptibility contrast (Rosen et al., 1990) or PET imaging (Leenders et al., 1990). The numerical values found in gray and white matter (CBV_GM=3.1±0.7%, CBV_WM=1.9±0.4%, n=5) agree with literature reports on PET (((Leenders et al., 1990), CBV_GM=4.3±0.8%, CBV_WM=2.7±0.6%, n=32), ((Grandin et al., 2005), CBV_GM=3.7±0.4%, CBV_WM=1.3±1.2%, n=13)) and MR reports using different approaches (((Srour et al., 2011), bookend technique, CBV_GM=3.4±0.6%, CBV_WM=1.5±0.3%, n=19), ((Bulte et al., 2007), hyperoxic challenge, CBV_GM=3.9±0.9%, CBV_WM=2.5±0.8%, n=6), ((Newman et al., 2003), T2*w and contrast infusion, CBV_GM=3.8±1.9%, CBV_WM=1.9±0.4%, n=6)). It further correlates with our results obtained using a steady-state susceptibility approach (note that steady-state and dynamic susceptibility contrast imaging give similar CBV maps with iron oxide contrast injection in humans (Christen et al., 2013)). The standard deviation of CBV values found in our study could be explained by the influence of age and body weight in cerebral blood volumes (Leenders et al., 1990; Wenz et al., 1996). Vessel diameter and blood oxygen saturation were found to be uniform across the brain. Values of vessel radius in gray matter (12.6±2.4μm) seem to be lower than values found with vessel size imaging approach ((Kiselev et al., 2005), 18±5μm) but higher than reports from high-resolution microscopy of cortical blood vessels ((Lauwers et al., 2008), about 4 μm). Yet, it is worth to notice that vessel size imaging and vessel radius imaging are not equivalent in theory (Troprès et al., 2001) and that microscopy imaging doesn't average data from the whole brain. Interestingly, our values seem to be closer to results found using MRI approaches that use hypercapnic challenge in combination with calibration curves ((Jochimsen et al., 2010), GM_VesselRad=13.4±1.7μm, n=4). The SO2 values in gray matter (59.5±4.7%) agree with literature reports using PET ((Leenders et al., 1990), SO2=61.5±5.6%, n=32) and correlate with MR phase oximetry measurements in the superior sagittal sinus (this study). Yet, the estimates for white matter parameters tend to be less consistent. The generally lower SNR of the MRI signal and lower CBV in white matter compared to gray matter is likely the major source of variability. Very low values of blood oxygenation at the interface of gray and white matter (see maps Fig5) are likely to be due to incorrect modeling of tissue substructures and warrants further investigation. Comparison with other imaging modalities, such as near infrared spectroscopy, should also help interpreting the results.

There are several limitations in the current implementation. First, the MR sequence used to acquire the fingerprints is based on a 2D Cartesian spin echo acquisition. This limits the coverage to several centimeters of axial coverage for an acquisition time of about 4 min. A 3D version that uses parallel imaging could provide higher SNR or higher slice resolution, which is expected to improve parameter estimates. Studies of the optimal number of echo time points for parameter estimations could also be useful to determine whether echo planar imaging sequences such as gradient and spin echo methods (Schmiedeskamp et al., 2011) offer benefit. In this study, only the magnitude of signal evolution was analyzed to create the fingerprints, whereas phase information was ignored. It has been shown that the phase evolution also contains valuable information about magnetic susceptibility (Duyn et al., 2007), orientation of myelin fibers (Liu, 2010), and oxygenation in large blood vessels (Haacke et al., 2010). Exploiting a complex signal would provide an additional measurement that can be readily used to fit the model. The optimal choice of echo time sampling and contrast dosage warrants further study. Indeed, it is possible that only a fraction of echoes give information about blood volume, blood oxygenation and vessel diameters altogether. Particularly, early time of spin dephasing during FID and spin echo formation have been shown to be of importance in quantitative BOLD imaging (Yablonskiy and Haacke, 1994). The duration of this regime is also dependent on blood magnetic susceptibility and main magnetic field strength. This could further improve the sensitivity of the fingerprints to the microvascular characteristics and help increase the precision in blood oxygenation

measurements that have a relatively low accuracy in our current implementation. Lastly, following previous works on blood oxygenation measurements with BOLD based MRI (An and Lin, 2000; He and Yablonskiy, 2007), we assumed that Hct was homogeneous in the brain. Yet, any variations of local Hct will affect linearly our measurements of blood oxygen saturation ($\Delta\chi = \Delta\chi_0$.Hct.(1 – SO2)) and lead to quantification errors.

In this first version of vascular fingerprinting, a simple dictionary was designed based on relatively simplistic models for blood vessels and oxygen distribution. Specifically, we modeled the blood vessels as straight cylinders, with no preferential directions, and with uniform oxygenation across the network, similar to those used in previous mathematical models. A generalization of the virtual voxels that take greater heterogeneity into account is typically easier to accomplish with numerical methods than analytical methods. As described in previous studies (Christen et al., 2010), the dipole approach used for magnetic field estimates allows the computation of realistic vascular networks without expense of computation time. Virtual voxels containing different fractions of veins, capillaries and arteries can be created. Until now, MR vessel size imaging has been limited to the study of small vessels (<100microns) because of theoretical assumptions on the diffusion regime (static dephasing regime and diffusion narrowing regime) and requirement of a large number of blood vessels. As our simulations take into account the full effect of water diffusion, it should be possible to derive vascular information about large blood vessels. For these experiments, the orientation of the blood vessels relative to the main magnetic field has to be incorporated into the numerical simulations. The point-spread function will have a significant influence on the signal evolution, and should also be taken into account (Sedlacik et al., 2007). The model can also be refined by incorporating hindered diffusion at the vessel walls or water exchange between compartments.

In presence of pathology, information about variation in water diffusion, e.g. derived from acquisition of apparent diffusion coefficient maps, will be important and the vascular dictionary will need to be extended accordingly. The dictionary could also be adapted to account for processes of angiogenesis or partial alterations of the vascular network by considering microvascular vessel tortuousity networks. While complex numerical simulations can be created, attention must however be paid to the uniqueness of the fingerprint. Indeed, several combinations of parameters can lead to very similar fingerprints or the signal modulations might not be sufficient to distinguish multiple solutions through the matching algorithm.

In our study, ferumoxytol was used to remove unwanted effects such as B0 inhomogeneities and spin-spin relaxation. The long half-life of iron oxide particles was also convenient to boost SNR. Yet, variations of magnetic susceptibility induced by gadolinium-based contrast agents might lead to similar results. The method could also be used to analyze acquisitions during bolus injections, giving more insight into dynamic processes such as blood flow and arterial delays. In fact, the numerical simulation tool has already been shown to be well adapted for dynamic contrast enhanced imaging (Pannetier et al., 2013a). Hyperoxic or hypercapnic challenges could be foreseen to induce variations of blood magnetic susceptibility. This will, however, require a different numerical modeling approach. In particular, effects of O2 or CO2 inhalation on vasodilation and vasorestriction have to be taken into account. SNR will be an issue, as O2 has small effects on blood magnetic susceptibility. In theory, perfusion fingerprinting could also be performed without contrast injection. While we showed that a dictionary using GESFIDE with T2 correction is unlikely to estimate SO2 and CBV because of crosstalk between the parameters (see Fig. 2a-c), other MR sequences might however be considered. In particular, balanced steady-state free precession (SSFP) with phase cycling has been shown to have good sensitivity to blood oxygenation changes (Miller et al., 2003). The fingerprints could also be created using other

combinations of multiple MR sequences, opening the way to a better comprehension of the MR exam.

Acknowledgments

Sources of Funding: This project was supported in part by National Institute of Health (2RO1NS047607, 1R01NS066506, 5P41RR09784, P41RR023953), the Lucas Foundation, the Oak Foundation, the National Center for Research Resources and with resources of the Veterans Affairs Medical Center, San Francisco, California.

References

An H, Lin W. Quantitative measurements of cerebral blood oxygen saturation using magnetic resonance imaging. J. Cereb. Blood Flow Metab. Off. J. Int. Soc. Cereb. Blood Flow Metab. 2000; 20:1225–1236.

Bandettini PA, Wong EC. Effects of biophysical and physiologic parameters on brain activation-induced R2* and R2 changes: Simulations using a deterministic diffusion model. Int. J. Imaging Syst. Technol. 1995; 6:133–152.

Bihan DL. Apparent Diffusion Coefficient and Beyond: What Diffusion MR Imaging Can Tell Us about Tissue Structure. Radiology. 2013; 268:318–322. [PubMed: 23882093]

Bulte D, Chiarelli P, Wise R, Jezzard P. Measurement of cerebral blood volume in humans using hyperoxic MRI contrast. J. Magn. Reson. Imaging JMRI. 2007; 26:894–899.

Carmeliet P, Jain RK. Angiogenesis in cancer and other diseases. Nature. 2000; 407:249–257. [PubMed: 11001068]

Christen T, Lemasson B, Pannetier N, Farion R, Remy C, Zaharchuk G, Barbier EL. Is t2* enough to assess oxygenation? Quantitative blood oxygen leveldependent analysis in brain tumor. Radiology. 2012; 262:495–502. [PubMed: 22156990]

Christen T, Lemasson B, Pannetier N, Farion R, Segebarth C, Rémy C, Barbier EL. Evaluation of a quantitative blood oxygenation level-dependent (qBOLD) approach to map local blood oxygen saturation. NMR Biomed. 2010

Christen T, Ni W, Qiu D, Schmiedeskamp H, Bammer R, Moseley M, Zaharchuk G. High-resolution cerebral blood volume imaging in humans using the blood pool contrast agent ferumoxytol. Magn. Reson. Med. 2013; 70:705–710.

Dennie J, Mandeville JB, Boxerman JL, Packard SD, Rosen BR, Weisskoff RM. NMR imaging of changes in vascular morphology due to tumor angiogenesis. Magn. Reson. Med. Off. J. Soc. Magn. Reson. Med. Soc. Magn. Reson. Med. 1998; 40:793–799.

Dickson JD, Ash TWJ, Williams GB, Sukstanskii AL, Ansorge RE, Yablonskiy DA. Quantitative phenomenological model of the BOLD contrast mechanism. J. Magn. Reson. San Diego Calif 1997. 2011; 212:17–25.

Duyn JH, van Gelderen P, Li T-Q, de Zwart JA, Koretsky AP, Fukunaga M. High-field MRI of brain cortical substructure based on signal phase. Proc. Natl. Acad. Sci. U. S. A. 2007; 104:11796–11801. [PubMed: 17586684]

Eichling JO, Raichle ME, Grubb RL Jr, Larson KB, Ter-Pogossian MM. In vivo determination of cerebral blood volume with radioactive oxygen-15 in the monkey. Circ. Res. 1975; 37:707–714. [PubMed: 811413]

Fernández-Seara MA, Techawiboonwong A, Detre JA, Wehrli FW. MR susceptometry for measuring global brain oxygen extraction. Magn. Reson. Med. Off. J. Soc. Magn. Reson. Med. Soc. Magn. Reson. Med. 2006; 55:967–973.

Grandin CB, Bol A, Smith AM, Michel C, Cosnard G. Absolute CBF and CBV measurements by MRI bolus tracking before and after acetazolamide challenge: Repeatabilily and comparison with PET in humans. NeuroImage. 2005; 26:525–535. [PubMed: 15907309]

Haacke EM, Tang J, Neelavalli J, Cheng YCN. Susceptibility mapping as a means to visualize veins and quantify oxygen saturation. J. Magn. Reson. Imaging JMRI. 2010; 32:663–676.

He X, Yablonskiy DA. Quantitative BOLD: mapping of human cerebral deoxygenated blood volume and oxygen extraction fraction: default state. Magn. Reson. Med. Off. J. Soc. Magn. Reson. Med. Soc. Magn. Reson. Med. 2007; 57:115–126.

Hunter JM, Kwan J, Malek-Ahmadi M, Maarouf CL, Kokjohn TA, Belden C, Sabbagh MN, Beach TG, Roher AE. Morphological and pathological evolution of the brain microcirculation in aging and Alzheimer's disease. PloS One. 2012; 7:e36893. [PubMed: 22615835]

Jochimsen TH, Ivanov D, Ott DVM, Heinke W, Turner R, Möller HE, Reichenbach JR. Whole-brain mapping of venous vessel size in humans using the hypercapnia-induced BOLD effect. NeuroImage. 2010; 51:765–774. [PubMed: 20188189]

Kiselev VG, Strecker R, Ziyeh S, Speck O, Hennig J. Vessel size imaging in humans. Magn. Reson. Med. Off. J. Soc. Magn. Reson. Med. Soc. Magn. Reson. Med. 2005; 53:553–563.

Klassen LM, Menon RS. NMR simulation analysis of statistical effects on quantifying cerebrovascular parameters. Biophys. J. 2007; 92:1014–1021. [PubMed: 17085487]

Krüger G, Kastrup A, Glover GH. Neuroimaging at 1.5 T and 3.0 T: comparison of oxygenation-sensitive magnetic resonance imaging. Magn. Reson. Med. Off. J. Soc. Magn. Reson. Med. Soc. Magn. Reson. Med. 2001; 45:595–604.

Lauwers F, Cassot F, Lauwers-Cances V, Puwanarajah P, Duvernoy H. Morphometry of the human cerebral cortex microcirculation: general characteristics and space-related profiles. NeuroImage. 2008; 39:936–948. [PubMed: 17997329]

Leenders KL, Perani D, Lammertsma AA, Heather JD, Buckingham P, Healy MJ, Gibbs JM, Wise RJ, Hatazawa J, Herold S. Cerebral blood flow, blood volume and oxygen utilization. Normal values and effect of age. Brain J. Neurol. 1990; 113(Pt 1):27–47.

Lindeberg T. Scale-space for discrete signals. IEEE Trans. Pattern Anal. Mach. Intell. 1990; 12:234–254.

Liu C. Susceptibility tensor imaging. Magn. Reson. Med. Off. J. Soc. Magn. Reson. Med. Soc. Magn. Reson. Med. 2010; 63:1471–1477.

Ma D, Gulani V, Seiberlich N, Liu K, Sunshine JL, Duerk JL, Griswold MA. Magnetic resonance fingerprinting. Nature. 2013; 495:187–192. [PubMed: 23486058]

Marques JP, Bowtell R. Application of a Fourier-based method for rapid calculation of field inhomogeneity due to spatial variation of magnetic susceptibility. Concepts Magn. Reson. Part B Magn. Reson. Eng. 2005; 25B:65–78.

McLeod, BC.; Szczepiorkowski, ZM.; Weinstein, R.; Winters, J. Apheresis: principles and practice. Bethesda, Md: AABB Press; 2010.

Miller KL, Hargreaves BA, Lee J, Ress D, deCharms RC, Pauly JM. Functional brain imaging using a blood oxygenation sensitive steady state. Magn. Reson. Med. Off. J. Soc. Magn. Reson. Med. Soc. Magn. Reson. Med. 2003; 50:675–683.

Newman GC, Delucia-Deranja E, Tudorica A, Hospod FE, Patlak CS. Cerebral blood volume measurements by T*2-weighted MRI and contrast infusion. Magn. Reson. Med. Off. J. Soc. Magn. Reson. Med. Soc. Magn. Reson. Med. 2003; 50:844–855.

Ogawa S, Lee TM, Kay AR, Tank DW. Brain magnetic resonance imaging with contrast dependent on blood oxygenation. Proc. Natl. Acad. Sci. U. S. A. 1990; 87:9868–9872. [PubMed: 2124706]

Otsu N. A threshold selection method from graylevel histograms. IEEE Trans Syst Madn Cybern. 1979; 9:62–66.

Pannetier NA, Debacker CS, Mauconduit F, Christen T, Barbier EL. A simulation tool for dynamic contrast enhanced MRI. PloS One. 2013a; 8:e57636. [PubMed: 23516414]

Pannetier NA, Sohlin M, Christen T, Schad L, Schuff N. Numerical Approach for quantitative BOLD with Vessel Size Estimate – Validation on Phantom. ISMRM 3121. 2013b

Rigau V, Morin M, Rousset M-C, de Bock F, Lebrun A, Coubes P, Picot M-C, Baldy-Moulinier M, Bockaert J, Crespel A, Lerner-Natoli M. Angiogenesis is associated with blood-brain barrier permeability in temporal lobe epilepsy. Brain J. Neurol. 2007; 130:1942–1956.

Rosen BR, Belliveau JW, Vevea JM, Brady TJ. Perfusion imaging with NMR contrast agents. Magn Reson Med. 1990; 14:249–265. [PubMed: 2345506]

Salomir R, de Senneville BD, Moonen CT. A fast calculation method for magnetic field inhomogeneity due to an arbitrary distribution of bulk susceptibility. Concepts Magn. Reson. B. 2003; 19:26–34.

Schmiedeskamp H, Straka M, Newbould RD, Zaharchuk G, Andre JB, Olivot J-M, Moseley ME, Albers GW, Bammer R. Combined spin- and gradient-echo perfusion-weighted imaging. Magn. Reson. Med. Off. J. Soc. Magn. Reson. Med. Soc. Magn. Reson. Med. 2011

Sedlacik J, Rauscher A, Reichenbach JR. Obtaining blood oxygenation levels from MR signal behavior in the presence of single venous vessels. Magn. Reson. Med. Off. J. Soc. Magn. Reson. Med. Soc. Magn. Reson. Med. 2007; 58:1035–1044.

Sedlacik J, Reichenbach JR. Validation of quantitative estimation of tissue oxygen extraction fraction and deoxygenated blood volume fraction in phantom and in vivo experiments by using MRI. Magn. Reson. Med. Off. J. Soc. Magn. Reson. Med. Soc. Magn. Reson. Med. 2010; 63:910–921.

Sobesky J, Zaro Weber O, Lehnhardt F-G, Hesselmann V, Neveling M, Jacobs A, Heiss W-D. Does the mismatch match the penumbra? Magnetic resonance imaging and positron emission tomography in early ischemic stroke. Stroke J. Cereb. Circ. 2005; 36:980–985.

Sohlin MC, Schad LR. Susceptibility-related MR signal dephasing under nonstatic conditions: experimental verification and consequences for qBOLD measurements. J. Magn. Reson. Imaging JMRI. 2011; 33:417–425.

Spees WM, Yablonskiy DA, Oswood MC, Ackerman JJ. Water proton MR properties of human blood at 1.5 Tesla: magnetic susceptibility, T(1), T(2), T*(2), and non-Lorentzian signal behavior. Magn. Reson. Med. Off. J. Soc. Magn. Reson. Med. Soc. Magn. Reson. Med. 2001; 45:533–542.

Srour JM, Shin W, Shah S, Sen A, Carroll TJ. SCALE-PWI: A pulse sequence for absolute quantitative cerebral perfusion imaging. J. Cereb. Blood Flow Metab. Off. J. Int. Soc. Cereb. Blood Flow Metab. 2011; 31:1272–1282.

Troprès I, Grimault S, Vaeth A, Grillon E, Julien C, Payen JF, Lamalle L, Décorps M. Vessel size imaging. Magn. Reson. Med. Off. J. Soc. Magn. Reson. Med. Soc. Magn. Reson. Med. 2001; 45:397–408.

Vaupel P, Mayer A. Hypoxia in cancer: significance and impact on clinical outcome. Cancer Metastasis Rev. 2007; 26:225–239. [PubMed: 17440684]

Wenz F, Rempp K, Brix G, Knopp MV, Gückel F, Heß T, van Kaick G. Age dependency of the regional cerebral blood volume (rCBV) measured with dynamic susceptibility contrast MR imaging (DSC). Magn. Reson. Imaging. 1996; 14:157–162. [PubMed: 8847971]

Yablonskiy DA, Haacke EM. Theory of NMR signal behavior in magnetically inhomogeneous tissues: The static dephasing regime. Magn. Reson. Med. 1994; 32:749–763. [PubMed: 7869897]

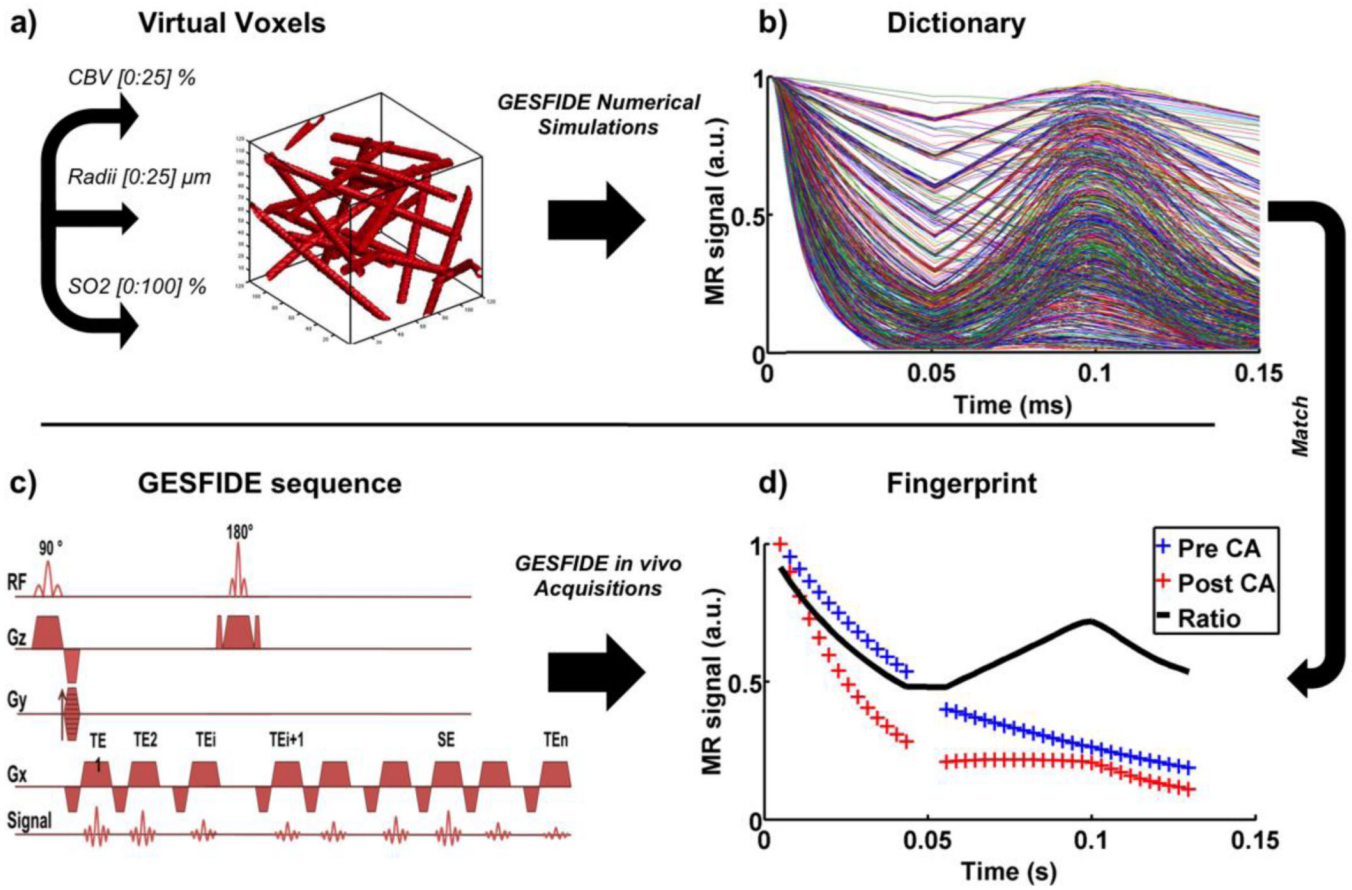

Figure 1.

Summary of MR vascular fingerprinting. (a) A numerical simulation with different parameters for CBV, vessel size (R), and oxygen saturation (SO2) is used to create a family of curves (the dictionary) (b). (c,d) The actual fingerprint derived from GESFIDE imaging is then compared to this dictionary to find the underlying parameters that make the best match.

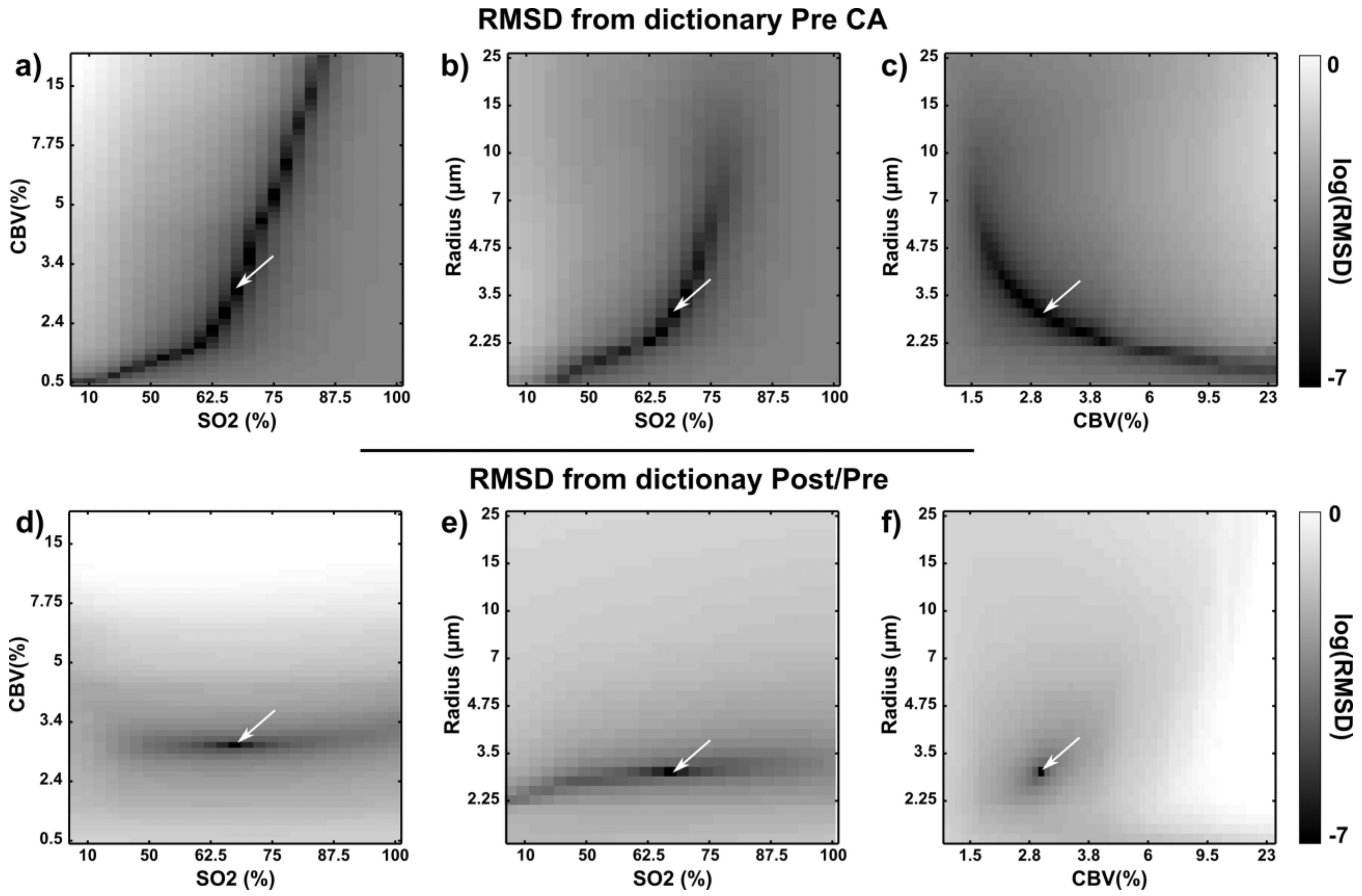

Figure 2.

Root mean square deviation plots illustrating the dissimilarity between a simulated reference MR signal (indicated by the white arrow) and the other simulated MR signals of the dictionary. Two dictionaries are investigated: The dictionary prior to the contrast agent injection (a-c) and the dictionary of the vascular fingerprint generated by the ratio Post/Pre contrast agent injection (d-f). Three orthogonal planes that intersect at the reference MR signal are represented. Large dispersions of minima (undesirable) are observed in the dictionary prior to contrast injection (a-c) whereas more localized minima (desirable) are noticed in the pre- and post-contrast ratio based vascular fingerprint dictionary (d-f). Note the non-linear scales.

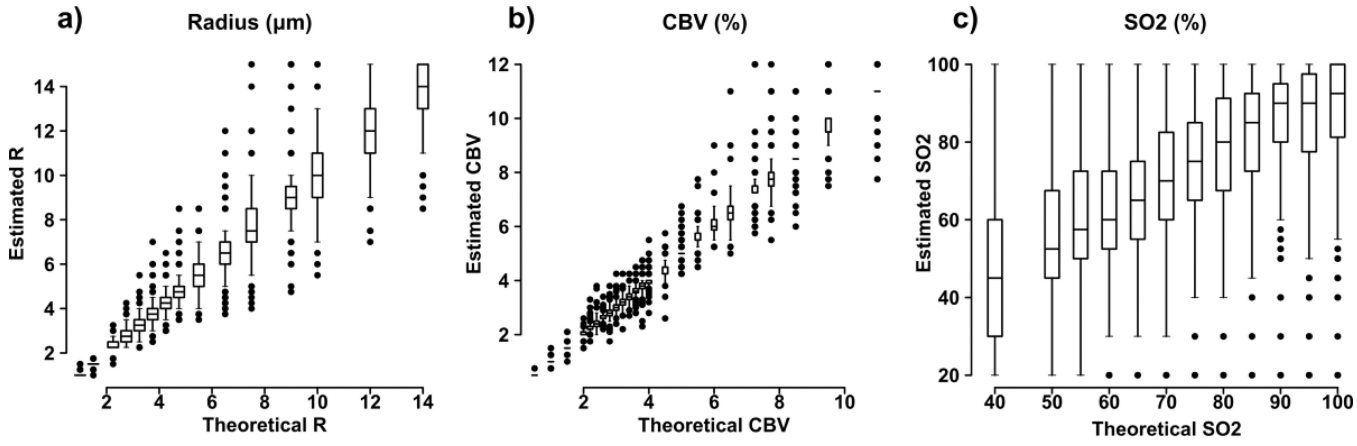

Figure 3.

Box-and-whisker plots illustrating the reliability of the vascular fingerprinting approach. Estimated R, CBV, and SO2 values are compared to their theoretical values. Linear trends are observed for all parameters. A lower accuracy is noticed in the SO2 estimates and to some extent in the estimates of radii compared to the CBV estimates (mean absolute relative error for SO2=21%, R=9%, and CBV=4%).

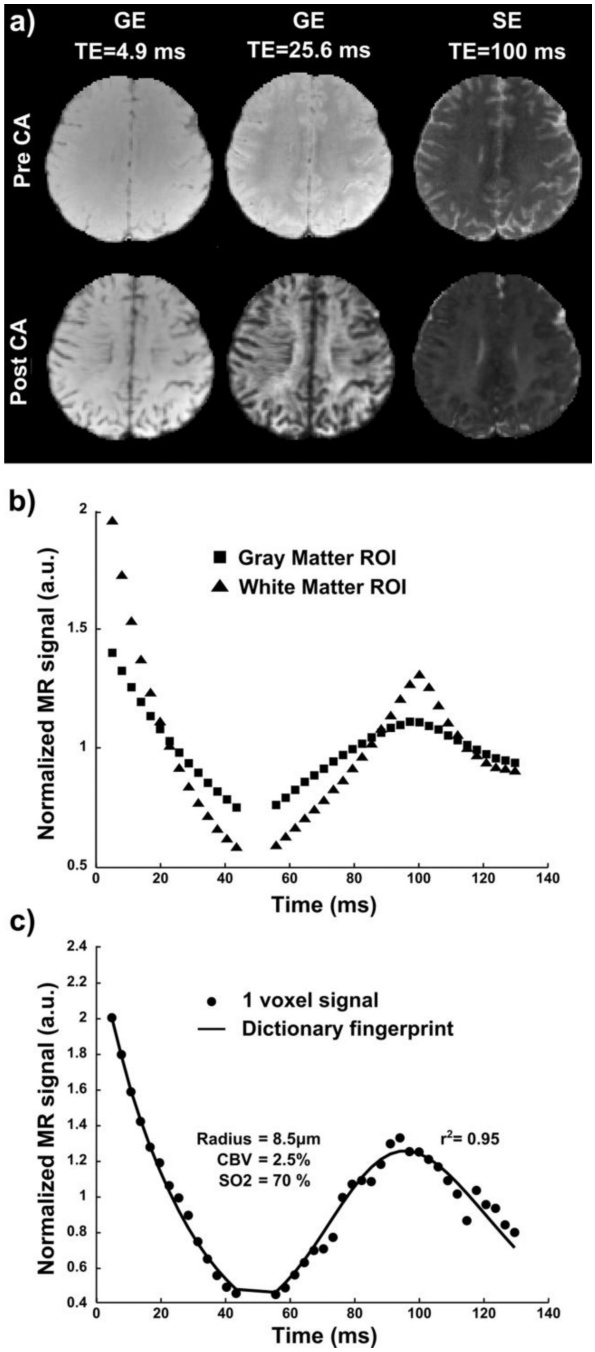

Figure 4.

a) GESFIDE images at TE=4.9ms and TE=25.6ms (GE) and at TE=100ms (SE) prior and after the contrast agent injection. b) Normalized vascular fingerprints averaged over the whole acquisition gray matter (square) and the white matter (triangles) volume. c) Example of the fingerprint for one voxel (dots) and its corresponding match from the dictionary (line).

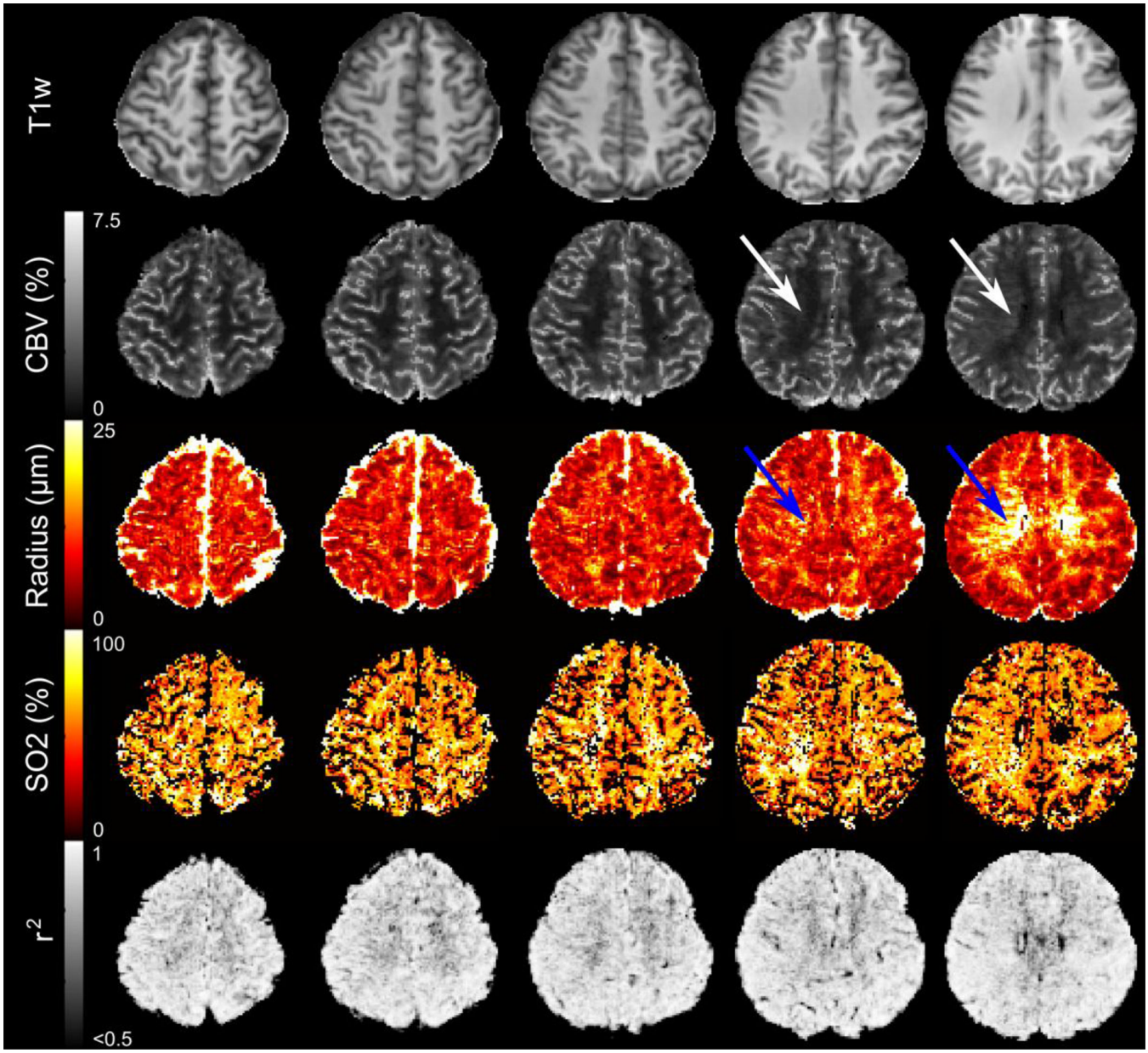

Figure 5.
Representative parametric maps obtained in volunteer #4 (who had the highest correlation coefficient for the match between the fingerprint and the dictionary). Voxel with $r^2 < 0.5$ are discarded. White and blue arrows indicate that the technique is sensitive enough to detect the relatively small medullary veins of the deep white matter.

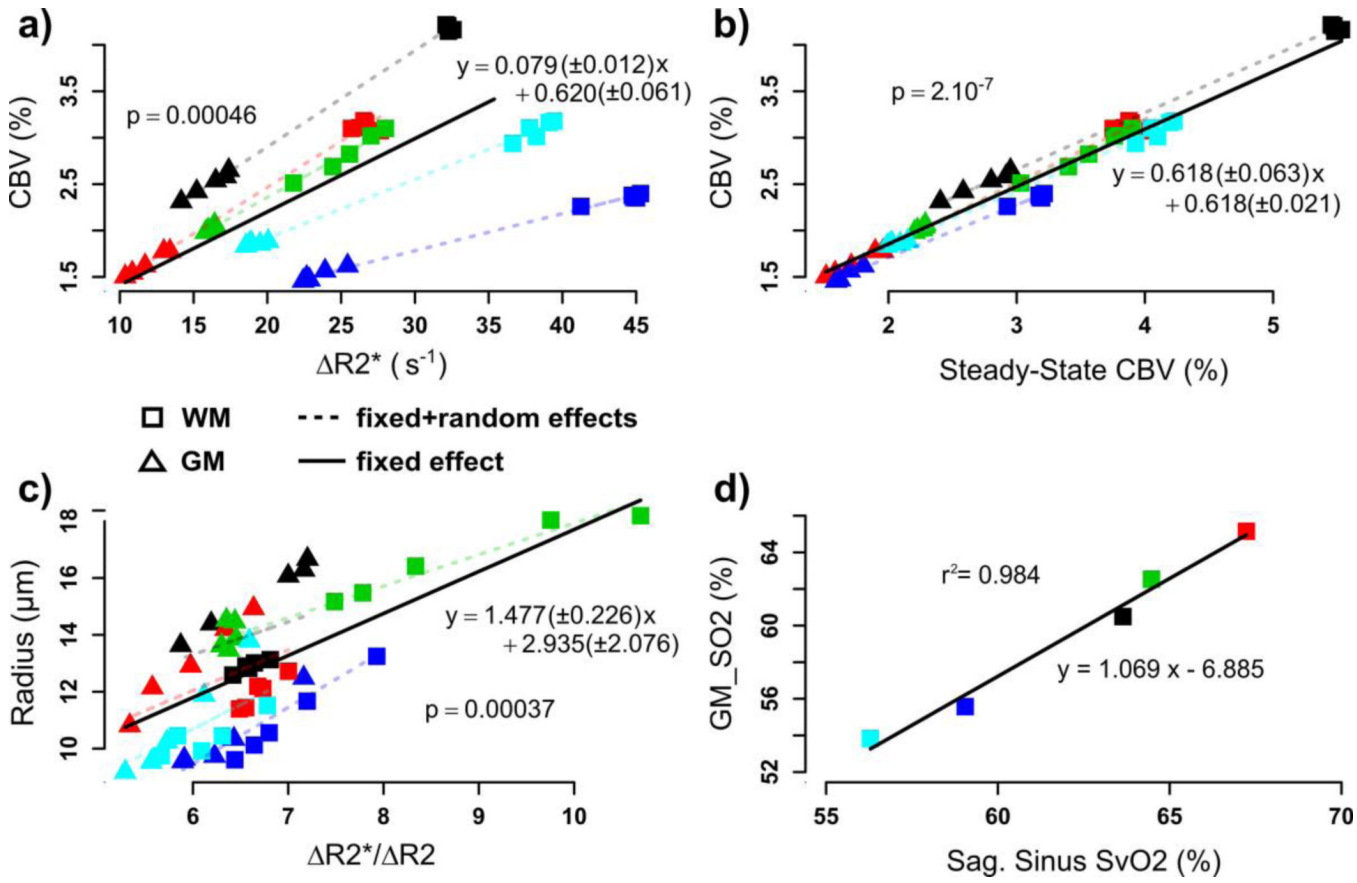

Figure 6.

Relationship between vascular measurements from the different methods evaluated from regions of interest in the whole white matter (squares) or grey matter (triangles) volumes in the normal subjects (n=5) and in each of the 5 slices. Each volunteer is identified by a different color. In (a-c), the equations of linear relations are derived from the fixed effect estimations. The level of significance is also listed. a) Relationship between ΔR2* (1/s) and CBV; b) steady-state CBV (%) and CBV; c) and ΔR2*/ΔR2 and R. d) Linear regression between global sagittal sinus SvO2 and SO2 in grey matter.

Table 1

Mean values of Radius, CBV, SO2 and the corresponding coefficient of determination (r^2 used as index of the goodness of the fits) obtained in the five volunteers in respectively gray and white matter.

Subject	Sex	Weight (kg)	Age	$\Delta\chi_{inj}$ (ppm)	Radius (μm)		CBV (%)		SO2 (%)		r^2	
					GM	WM	GM	WM	GM	WM	GM	WM
1	M	100	27	0.17	12.9	15.4	4.2	2.5	60.5	50.2	0.8	0.7
2	M	86	27	0.20	12.0	13.0	3.1	1.6	65.1	48.1	0.8	0.7
3	M	82	61	0.21	16.6	14.0	2.8	2.0	62.5	57.6	0.8	0.8
4	F	45	30	0.42	11.0	10.3	2.3	1.5	55.6	56.4	0.9	0.9
5	F	68	34	0.28	10.4	10.9	3.1	1.9	53.8	52.7	0.8	0.8
Average		**76**	**37**	**0.26**	**12.6**	**12.7**	**3.1**	**1.9**	**59.5**	**53.0**	**0.8**	**0.8**
Std		**21**	**14**	**0.10**	**2.4**	**2.1**	**0.7**	**0.4**	**4.7**	**4.0**	**0.0**	**0.1**